

# Conversion of Aminodeoxychorismate Synthase into Anthranilate Synthase with Janus Mutations: Mechanism of Pyruvate Elimination Catalyzed by Chorismate Enzymes

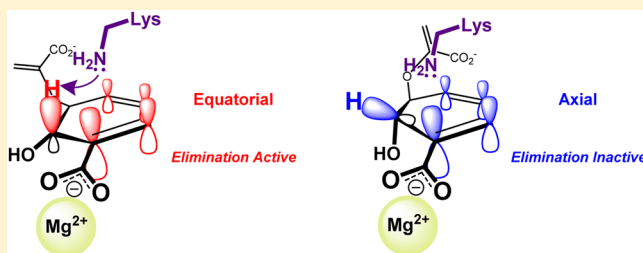
Justin E. Culbertson,<sup>†</sup> Dong hee Chung,<sup>†</sup> Kristin T. Ziebart,<sup>‡</sup> Eduardo Espiritu,<sup>§</sup> and Michael D. Toney<sup>\*,†</sup>

<sup>†</sup>Department of Chemistry, University of California, Davis, Davis, California 95616, United States

<sup>‡</sup>Department of Chemistry, Oregon State University, Corvallis, Oregon 97331-4003, United States

<sup>§</sup>Department of Chemistry and Biochemistry, Arizona State University, Tempe, Arizona 85287, United States

**ABSTRACT:** The central importance of chorismate enzymes in bacteria, fungi, parasites, and plants combined with their absence in mammals makes them attractive targets for antimicrobials and herbicides. Two of these enzymes, anthranilate synthase (AS) and aminodeoxychorismate synthase (ADCS), are structurally and mechanistically similar. The first catalytic step, amination at C2, is common between them, but AS additionally catalyzes pyruvate elimination, aromatizing the aminated intermediate to anthranilate. Despite prior attempts, the conversion of a pyruvate elimination-deficient enzyme into an elimination-proficient one has not been reported. Janus, a bioinformatics method for predicting mutations required to functionally interconvert homologous enzymes, was employed to predict mutations to convert ADCS into AS. A genetic selection on a library of Janus-predicted mutations was performed. Complementation of an AS-deficient strain of *Escherichia coli* grown on minimal medium led to several ADCS mutants that allow growth in 6 days compared to 2 days for wild-type AS. The purified mutant enzymes catalyze the conversion of chorismate to anthranilate at rates that are ~50% of the rate of wild-type ADCS-catalyzed conversion of chorismate to aminodeoxychorismate. The residues mutated do not contact the substrate. Molecular dynamics studies suggest that pyruvate elimination is controlled by the conformation of the C2-aminated intermediate. Enzymes that catalyze elimination favor the equatorial conformation, which presents the C2-H to a conserved active site lysine (Lys424) for deprotonation and maximizes stereoelectronic activation. Acid/base catalysis of pyruvate elimination was confirmed in AS and salicylate synthase by showing incorporation of a solvent-derived proton into the pyruvate methyl group and by solvent kinetic isotope effects on pyruvate elimination catalyzed by AS.



The shikimate biosynthetic pathway is used by bacteria, fungi, algae, plants, and many eukaryotic parasites (e.g., *Plasmodium falciparum*) to connect carbohydrate and aromatic metabolism. The end product of the shikimate pathway, chorismate, is the common precursor for carbocyclic aromatic compounds in biological systems.<sup>1–3</sup> The shikimate pathway itself is the target of glyphosate, the most successful herbicide in agriculture.<sup>2</sup> Pathways that begin with chorismate are also excellent targets for herbicides and antimicrobials.

Anthranilate synthase (AS) and 4-amino-4-deoxychorismate synthase (ADCS) catalyze the first steps of tryptophan and folate biosynthesis, respectively, starting from chorismate. These pathways are required for survival by plants and free-living microorganisms, and infectious bacteria require them for virulence.<sup>3,4</sup> Folate metabolism is a proven target for antibacterials, being the target of the sulfa drugs and trimethoprim. The production of 4-amino-4-deoxychorismate (ADC) by ADCS is also important to secondary metabolic pathways that produce the antibiotics candididin, chloramphenicol, and pristinamycin.<sup>3</sup>

AS and ADCS are structurally homologous and have a two-domain  $\alpha/\beta$  fold. Their active sites are highly conserved, as are

those of other enzymes in this family (Figure 1).<sup>5–9</sup> AS converts chorismate to anthranilate (2-aminobenzoate) in a two-step process: (1) amination of chorismate at C2 to form 2-amino-2-deoxyisochorismate (ADIC) as an enzyme-bound intermediate and (2) elimination of pyruvate from ADIC to form anthranilate. ADCS, like AS, requires ammonia to aminate chorismate, but unlike AS, it does not catalyze elimination of the enolpyruvyl group of ADC (Figure 2). Interestingly, although the elimination of the enolpyruvyl group is the next step in the biosynthesis of *p*-aminobenzoate, a second, pyridoxal phosphate-dependent enzyme (ADC lyase) is required.<sup>10</sup> ADCS can produce ADIC, the intermediate in the AS-catalyzed reaction, when a single mutation (K274A) is incorporated, but the mutant does not catalyze pyruvate elimination.<sup>11</sup>

AS and ADCS require amidotransferases that hydrolyze L-glutamine to L-glutamate and deliver the ammonia to the

Received: January 5, 2015

Revised: February 20, 2015

Published: February 24, 2015

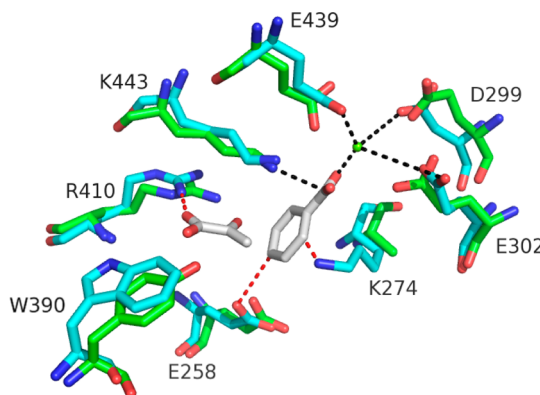


**Figure 1.** Overlay of *Serratia marcescens* AS (green) and *Escherichia coli* ADCS (blue) active sites. Pyruvate, benzoate, and  $Mg^{2+}$  were cocrystallized with AS. Residues are numbered according to the ADCS sequence.

chorismate active site via a tunnel in the protein interior, a common mechanism for avoiding free intracellular ammonia.<sup>11–16</sup> In the absence of L-glutamine or an amidotransferase subunit, AS and ADCS can employ ammonium salts as an ammonia source.

Other chorismate enzymes such as IS, ADIC synthase, and SS are structurally homologous, are  $Mg^{2+}$ -dependent, and catalyze a similar  $S_N2''$  nucleophilic substitution reaction (Figure 2).<sup>1,13,17–19</sup> AS, ADCS, and ADIC synthase (PhzE) use ammonia as a nucleophile, while IS and SS use water. The nucleophilic substitution mechanism is conserved among these four enzymes; however, only AS and SS possess pyruvate lyase activity.<sup>13</sup>

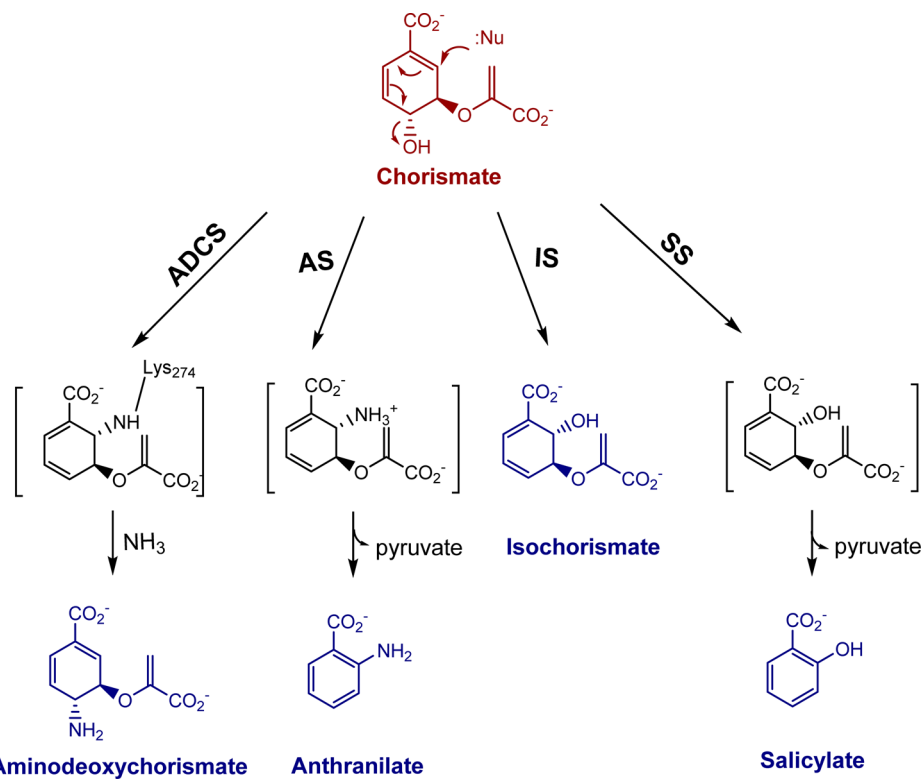


**Figure 2.** Previously proposed mechanism of the structurally homologous chorismate enzymes ADCS, AS, SS, and IS. Reactions are initiated by addition of either a nitrogen or an oxygen nucleophile at C2 with acid-catalyzed loss of the hydroxyl group at C4. AS and SS have pyruvate lyase activity, while ADCS and IS do not catalyze enolpyruvyl side chain elimination and aromatization.

The mechanism of pyruvate elimination in AS and SS continues to be debated. On the basis of isotopic experiments, two groups independently concluded more than 40 years ago that AS does not catalyze an intramolecular pericyclic proton transfer from C2 of the cyclohexadienyl ring to the enolpyruvyl methine carbon of ADIC to form anthranilate.<sup>20,21</sup> They proposed that pyruvate elimination proceeds via an acid/base mechanism (Figure 3). Mutagenesis studies of AS indicated

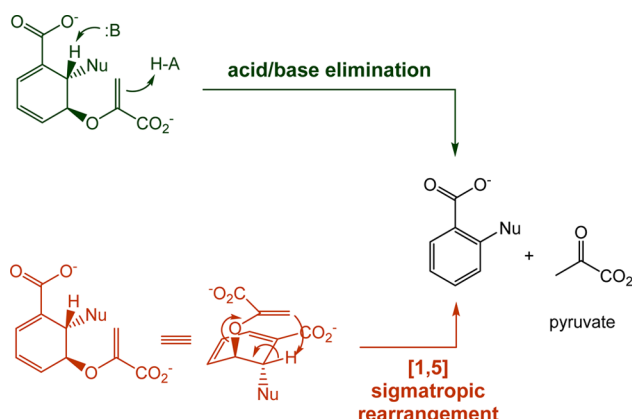


**Figure 3.** Alternative mechanisms for pyruvate elimination.

His398 might act as the general base, and Tyr449 was later proposed to be the general acid that protonates the enolpyruvyl methine carbon.<sup>1,6</sup> However, with the recent availability of scores of new enzyme sequences, the roles of His398 and Tyr449 in the AS elimination mechanism were questioned.<sup>8</sup> Comparisons of the structures of AS, ADCS, IS, and SS and the

sequences of more than 1000 enzymes did not reveal active site residues unique to AS and SS that could account for an acid/base elimination mechanism. Additionally, <sup>1</sup>H NMR work suggested that SS possesses promiscuous chorismate mutase activity in the absence of Mg<sup>2+</sup>.<sup>8</sup> Zwahlen et al. therefore concluded that AS and SS are mechanistically homologous to PchB, an isochorismate pyruvate lyase found in *Pseudomonas* sp. that is homologous to chorismate mutase, and that pyruvate elimination proceeds via a [1,5] sigmatropic rearrangement (Figure 3). However, Ziebart et al. showed that sufficient enzyme purification removes genuine chorismate mutase contamination, devaluing the mechanistic analogy.<sup>22</sup>

Herein, we report ADCS mutants that gain pyruvate lyase activity through the incorporation of mutations predicted by Janus, a computational method for ranking mutations for functional interconversion of enzymes.<sup>23</sup> Three of these mutant enzymes were purified and shown to have catalytic activities nearly identical to that of wild-type ADCS-catalyzed ADC formation. Computational analyses of enzyme–substrate complexes suggest that these enzymes direct pyruvate elimination by controlling the conformation of the bound 2-amino-2-deoxyisochorimate intermediate, and isotopic experiments provide supporting experimental evidence.

## MATERIALS AND METHODS

**Materials.** Terrific Broth II was purchased from MB biomedicals. Chorismate was prepared according to a literature procedure.<sup>13,24</sup> Oligonucleotides were purchased from Life Technologies. All other chemical reagents were purchased from either Fisher Scientific or Sigma-Aldrich and used without further purification.

**Janus Prediction of Mutations To Convert ADCS to AS.** Confirmed ADCS and AS sequences were compiled by performing BLAST searches of the Swiss-Prot database with *Escherichia coli* ADCS and *Serratia marcescens* AS sequences as search queries. Approximately 30 annotated bacterial sequences for each ADCS and AS were aligned with COBALT from the NCBI. Hidden Markov models were generated representing the ADCS and AS alignments with HMMER 3.0. The hidden Markov models were used to search the UniRef90 protein sequence database to build larger sequence sets for Janus input. In the end, 50 sequences for each enzyme were aligned using COBALT and subsequently used. Janus version 16.6 was used to generate predictions, using *E. coli* ADCS as the reference sequence. Protein Data Bank (PDB) entry 1K0E was used as the reference structure. Atom 2210 (NZ of K274) was used for measuring distances from the active site.

**Library Construction and Selection.** PCR-amplified *pabB*-K274A was digested with 0.6 unit of DNaseI (NEB) in a 200  $\mu$ L reaction mixture containing 100 mM Tris-HCl (pH 7.4) and 1 mM MnCl<sub>2</sub> for 5 min at 15 °C, followed by DNaseI inactivation at 90 °C for 10 min. Fragments of approximately 50–150 bp were purified from a 2.5% low-melting agarose gel with a Takara Recochip (Takara Bio, Inc.) followed by removal of ethidium bromide by a Centri-Sep desalting column (Princeton Separations).

Synthetic 50 bp oligonucleotides containing the top 15 Janus-predicted conservation-based mutations and purified *pabB* K274A fragments were combined in an equimolar ratio in a PCR mixture (dNTPs at 200  $\mu$ M each, 1× *Pfu* DNA polymerase reaction buffer, 100 ng of total oligonucleotide, and fragment mixture), and 2.5 units of *Pfu*Turbo DNA polymerase (Stratagene) was added per 100  $\mu$ L reaction mixture. The

following thermocycler program was used for gene reassembly: 94 °C for 5 min followed by 45 cycles of 94 °C for 1 min, 52 °C for 1 min, and 72 °C for 1 min, and finally 72 °C for 10 min. The assembled product was amplified by conventional PCR using the following primers: fwd, 5'CGATGACGATAAGGATCGATGGG3'; rev, 5'GAAAATCTTCTCATCCGCAAAAC3'. The amplified library and pBAD vector were digested with restriction enzymes *Xba*I and *Hind*III and ligated with T4 DNA ligase at a 10:1 insert:vector ratio.

Ligations were transformed into *E. coli* JW1256-1 cells from the Keio knockout collection [genotype *F*,  $\Delta$ (*araD*-*araB*)S67,  $\Delta$ *lacZ4787*(::*rmB*-3),  $\lambda$ ,  $\Delta$ *trpE772*::*kan*, *rph*-1,  $\Delta$ (*rhaD*-*rhaB*)S68, *hsdR514*] by electroporation. Cells were rescued after electroporation with SOC medium without antibiotic for 1 h at 37 °C while being shaken. Prior to being plated, the cells were pelleted at 1000g for 5 min; the supernatant was aspirated, and the pellet was gently resuspended in warm M9 minimal medium with 0.4% (w/v) glucose, re-centrifuged, and resuspended to remove excess Trp from the SOC medium. For selection of active clones, transformants were plated on selective medium and incubated at 37 °C for up to 14 days with a water reservoir in the incubator to prevent drying of the plates. Selective medium consisted of M9 salts with 15 g/L agar, 0.4% (w/v) glucose, 0.02% (w/v) L-arabinose, 50 mg/L kanamycin, 100 mg/L ampicillin, and each of the 20 standard amino acids except Trp (at 50 mg/L). Active clones were assigned growth times for the appearance of colonies at 24 h intervals. *E. coli* JW1256-1 alone and JW1256-1 containing pBAD with either *pabB*-K274A or *pabB*-WT were used as controls; none was unable to produce colonies on this medium during a 14 day incubation.

The procedure described above produced only three isolates capable of growing on selective medium. Therefore, different procedures were used to make two additional libraries for mutant isolation. In the first library, the five invariant mutations from the first round were mixed and matched to test their individual contributions to activity. PCR-amplified *pabB* was used as a template for a PCR mixture that contained 1× Phusion HF buffer, dNTPs (200  $\mu$ M each), 0.1  $\mu$ M oligonucleotides containing each of K274A, L277R, N303H, F334Y, and C391G mutations, and forward and reverse end primers that include 20 bp of sequence complementary to the template gene and 20 bp complementary overhangs to the pBAD cloning region near *Xba*I and *Hind*III restriction sites for use in Gibson cloning. End primer sequences were as follows: fwd, 5'CGATGGGATCCGAGCTCGAGATGAAGACGTT-ATCTCCGCTGTG3'; rev, 5'TCCGCCAAACAGCCAA-GCTTTAACCTCTCCAGTTGCTTCAGGAT3'. During the reaction, random fragments of DNA are synthesized and act as megaprimer for subsequent rounds of PCR. The megaprimer are fully extended by annealing onto a template or other megaprimer. The products can serve as a template for mutant primers in subsequent cycles. The final products of the reaction contain a mixture of mutant megaprimer and reassembled mutant *pabB*. The reaction products were purified using DNA Clean & Concentrator (Zymo Research). The purified DNA was used as a template to generate the fully reassembled *pabB* library using identical PCR conditions with the overhang end primers but no mutant oligonucleotides. The thermocycler program used for reassembly was 98 °C for 3 min, and 30 cycles of 98 °C for 10 s, 67 °C for 20 s, and 72 °C for 30 s, and finally 72 °C for 7 min. The reassembled library was sequenced to confirm incorporation of all five point mutations. Gibson

cloning was used to introduce the amplified library into the pBAD vector. The Gibson reaction mixture was heat inactivated in a thermocycler at 65 °C for 1 h, followed by transformation and selection as described above.

In the second library, 15 individual PCRs with primers containing individual Janus-predicted mutations were performed to synthesize mutant megaprimer. These megaprimer were mixed together with wild-type template and randomly reassembled in a single PCR mixture using the end primers given above, generating a library of *pabB* with mixed-and-matched Janus-predicted point mutations (Table 1). The last

**Table 1. Janus Mutation Predictions for the ADCS-to-AS Conversion<sup>a</sup>**

conservation		covariation		
score <sup>b</sup>	predicted change	score <sup>b</sup>	predicted change	basis <sup>c</sup>
100	K274A	100	G425A	polarity: 425
85	N213V	80	M310A	polarity: 310, 380
57	I367L	80	W390Y	polarity: 390, 13
51	S366T	69	T270I	polarity: 270, 36
50	C391G	69	T408V	polarity: 408, 36
43	G364M	69	A361C	polarity: 361, 13
42	L214P	68	S406C	polarity: 335, 425
40	N303H	68	P335S	polarity: 338, 370
32	D299E	67	H338M	polarity: 338, 370
31	I306L	67	S393A	polarity: 393, 383
30	L277R	65	R300L	volume: 300, 122
28	R259S	65	V200L	polarity: 200, 13
27	P363N	64	L204I	polarity: 204, 122
25	G425A	64	F441R	polarity: 441, 195
23	F334Y	63	P42K	polarity: 42, 258

<sup>a</sup>Scores are distance-weighted and normalized to a range between 0 and 100. <sup>b</sup>Normalized to a scale of 0–100. <sup>c</sup>The basis for covariation includes the correlated property (polarity, volume, or hydrophilicity) and the correlated residue pair.

two libraries were constructed to provide coverage better than that achieved in the gene reassembly method described above. These megaprimer methods will be described in detail in a future manuscript.

**Protein Expression and Purification.** The preparation of SS has been described previously.<sup>22</sup> For AS, overnight cultures containing pBAD-2.6.1, pBAD-6.6.1, pBAD-7.6.1, pBAD-*trpE*, and pBAD-*pabB* K247A were grown in shaker flasks with 0.5 L of LB for ~3 h to an OD<sub>600</sub> of 1.0 with 50 µg/mL kanamycin and 100 µg/mL ampicillin. The shaker flasks were removed and cooled on ice for 30 min. Enzyme production was induced by adding L-arabinose to a final concentration of 0.2% (w/v), and the flasks were further incubated at 18 °C for 24 h. Approximately 5 g of cell paste was collected. Cells were collected by centrifugation at 3700g for 30 min, resuspended in lysis buffer [1× PBS, 1 mM MgCl<sub>2</sub>, 1 mM β-mercaptoethanol, and 10 mM imidazole (pH 7.4)], and disrupted by sonication. Insoluble material was removed by centrifugation at 3700g for 1 h. The soluble extracts were filtered through a 0.8 µm membrane. The proteins were purified over 250 µL of HisPur Cobalt Resin (Thermo) and eluted from the column using lysis buffer with 200 mM imidazole. After elution, the proteins were concentrated using vivaspin 20 concentrators. Approximately 2–5 mg of ~90% pure protein, verified by sodium dodecyl sulfate–polyacrylamide gel electrophoresis (SDS–PAGE), was produced from the initial purification. The enzymes were

additionally purified using FastQ anion exchange resin. Enzymes were loaded on a 1 mL gravity column equilibrated with starting buffer (1× PBS, 1 mM MgCl<sub>2</sub>, 1 mM β-mercaptoethanol, and 10 mM KCl) and eluted with a gradient to 200 mM KCl in starting buffer. The enzymes were subsequently concentrated with yields of 0.5–1 mg of >95% pure protein, confirmed by SDS–PAGE. Pure samples were dialyzed against PBS (pH 7.4), 50 mM KCl, 1 mM MgCl<sub>2</sub>, and 10 mM β-mercaptoethanol for 24 h. Protein concentrations were determined using the calculated molar extinction coefficient and the measured absorbance at 280 nm. Samples of 50 µL were flash-frozen and stored at –80 °C.

**Activity Assays.** Steady-state kinetics were performed on a BioTEK plate reader at 25 °C. Reactions of the three mutants and PabB K274A were conducted in 100 mM triethanolamine hydrochloride (TEA-HCl) (pH 7.8), 100 mM (NH<sub>4</sub>)<sub>2</sub>SO<sub>4</sub>, 5 mM MgCl<sub>2</sub> with 10–500 µM chorismate, and 40 nM enzyme. PabA was present at a concentration of 80 nM in reaction mixtures that included it. Reactions of TrpE or TrpEG (purified as described previously<sup>22</sup>) were conducted in 100 mM TEA-HCl (pH 7.8), 100 mM (NH<sub>4</sub>)<sub>2</sub>SO<sub>4</sub> or 20 mM L-glutamine, 5 mM MgCl<sub>2</sub> with 0.1–80 µM chorismate, and 2 nM enzyme. Anthranilate fluorescence ( $\lambda_{\text{ex}} = 313$  nm;  $\lambda_{\text{em}} = 390$  nm) was monitored in all reactions. Kinetic data were analyzed using Kalidagrap 3.6.

**High-Performance Liquid Chromatography (HPLC) Analysis.** The standard reaction mixture for HPLC analysis contained 100 mM TEA-HCl (pH 7.8), 100 mM (NH<sub>4</sub>)<sub>2</sub>SO<sub>4</sub>, 5 mM chorismate, 5 mM MgCl<sub>2</sub>, and 8 µM enzyme in a total volume of 150 µL. After 4 h at room temperature, the samples were ultrafiltered to remove protein and injected onto an Agilent 1100 HPLC system. Conditions for control reactions (no enzyme) were identical. A 5 µm Supelco Supelcosil C18 column (4.6 mm × 250 mm) was used to separate reaction mixtures. Mobile phase A was 5% acetic acid in water; mobile phase B was acetonitrile. Reaction mixtures were eluted with 95% A and 5% B for 5 min, followed by a gradient from 5 to 50% B from 5 to 20 min and then to 50% B from 20 to 25 min. Two detectors were used. The first monitored absorbance at 280 nm, while the second monitored fluorescence emission at 400 nm from excitation at 300 nm. The flow rate was 0.8 mL/min.

**<sup>1</sup>H NMR Analysis.** D<sub>2</sub>O (99.9%) was used to prepare solutions and to bring the final reaction volume to 0.90 mL. AS reaction mixtures contained 20 mM potassium phosphate (pD 7.8), 5 mM MgCl<sub>2</sub>, 100 mM (NH<sub>4</sub>)<sub>2</sub>SO<sub>4</sub>, 6 mM chorismate, and 20 µM enzyme. SS reaction mixtures contained 20 mM potassium phosphate (pD 7.8), 1 mM MgCl<sub>2</sub>, 6 mM chorismate, and 20 µM enzyme. AS and SS stock solutions were in H<sub>2</sub>O and contributed 21% (AS) and 30% (SS) by volume to the reaction mixtures. Control reactions were performed in which enzyme was replaced with D<sub>2</sub>O, and in which chorismate was replaced with 6 mM anthranilate (AS) or salicylate (SS) with 6 mM pyruvate. The conditions for these control reactions were otherwise identical to those described above. After 4 h at room temperature, samples were ultrafiltered to remove protein and analyzed on a Varian INOVA 600 MHz spectrometer. The PRESAT gradient spin echo sequence was used for solvent suppression, and the probe was tuned to D<sub>2</sub>O.

**Stopped Flow.** An Applied Photophysics SX-18MV stopped-flow instrument was used. The reaction mixtures contained 50 µM AS, 40 µM chorismate, 50 mM potassium

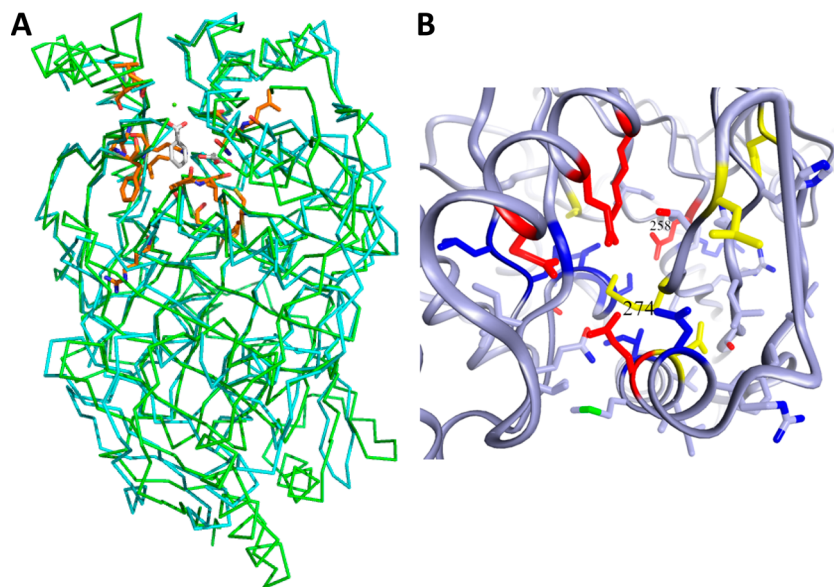


**Figure 4.** (A) Structural overlay of *S. marcescens* AS (green) and *E. coli* ADCS (blue) with Janus-predicted mutation sites (orange). Pyruvate, benzoate (gray), and  $Mg^{2+}$  (green sphere) were cocrystallized with AS. (B) Active site region of ADCS with Janus-predicted mutation sites. Mutations colored yellow were found in all three mutants isolated in the initial round of selection; other mutations are colored blue. Residues colored red are conserved catalytically critical residues common to both enzymes. Residues 274 and 258 are labeled for orientation. The view is from the top of the figure in panel A.

phosphate (pH/pD 7.0), 5 mM  $MgCl_2$ , and 20 mM L-glutamine and the reactions conducted at 25 °C. The anthranilate excitation wavelength was 313 nm, and emission above 340 nm was monitored with a long-pass filter. AS was dialyzed into  $D_2O$  before being used. The  $D_2O$  concentration was ~95% in the final reaction mixtures. Identical reaction conditions were used for SS, except excitation was at 300 nm and L-glutamine was not included.

**Computational Methods.** YASARA version 13.4.21 was used for molecular dynamics calculations.<sup>25–27</sup> Gaussian09W (version 8.0) was used for *ab initio* calculations. Chem3D Pro (version 13.0) was used for conformational analysis of chorismate and derivatives.

X-ray structures for ADCS (PDB entry 1K0E), AS (PDB entry 1I7Q), ADIC synthase (PDB entry 3R76), IS (PDB entry 3HWO), and SS (PDB entry 2FN1) were retrieved from the RCSB PDB. YASARA was used to model the K274A mutant of ADCS. The axial and equatorial conformations of the appropriate products (ADIC for AS, the K274A mutant of ADCS, and ADIC synthase; isochorismate for SS and IS) were modeled into the active sites of these enzymes based on the active site ligands present in the crystal structures. The enzyme–substrate complexes were subjected to simulated annealing energy minimization using YASARA. Crystallographic waters were kept (except those with steric clashes with modeled substrate), and additional waters were included to fill the cubic simulation cell that extended 10 Å beyond all protein atoms. The AMBER03 force field was used with a 1 fs time step. YASARA includes an automated procedure based on semiempirical AM1 calculations that assigns force field parameters to nonstandard residues such as chorismate and its derivatives. The correctness of these parameters was analyzed by performing simulated annealing on the isolated molecule and then manually checking bond lengths and angles. The enzyme–substrate complexes were temperature equilibrated for 25 ps at 298 K and then slowly cooled to 10 K over

100 ps. This was followed by steepest descent energy minimization.

The initial conformations of chorismate and its derivatives used for calculation of the conformational energy differences in Table 4 were obtained using the dihedral driver function in Chem3D Pro with the MM2 force field. The enolpyruvyl carboxylate group was protonated for these initial calculations. The structures obtained from this procedure were used directly as input for Gaussian09 energy minimization calculations using HF/6-311+G(d,p) with the PCM solvent model for water and methanol. The differences in energies between the corresponding axial and equatorial conformations are reported in Table 4.

## RESULTS

**Janus-Predicted Mutations.** Janus predictions for the ADCS to AS conversion are listed in Table 1 and shown pictorially in Figure 4. Because G425A is the only joint prediction between the conservation and covariation procedures in the 15 top-ranked predictions, the conservation mutations alone were used to generate a reasonably small library, allowing better coverage using the genetic selection. Previous work showed that the K274A mutation (K274 is conserved in ADCS, and the same residue is conserved as Ala in AS) was sufficient to convert ADCS into an ADIC synthase.<sup>11</sup>

**Selection for Active Mutants.** The selection for AS activity was based on the arabinose-inducible vector pBAD (Invitrogen) and an anthranilate synthase-deficient strain of *E. coli*. The *pabB*-K274A and *trpE* genes were also subcloned into pBAD. Determination of the growth time of pBAD-*pabB*-K274A in the selection strain used M9 selection plates with either 0.5  $\mu$ M anthranilate or Trp added. The two controls had similar growth times of 24 h.

The gene reassembly library produced ~3000 colonies per transformation. Twenty transformations were performed to give ~60000 total transformants, which covered the library ~3-fold. *E. coli* JW1256-1 transformed with pBAD-*pabB*-K274A shows no growth over 14 days on selection plates. *E. coli*

Table 2. Mutations Observed in Isolated Mutants<sup>a</sup>

growth <sup>b</sup>	2.6.1	6.6.1	7.6.1	H1-1	H1-2	H1-3	H1-4	H1-5	H1-6	H1-7	H1-8	H2-1	H2-3	H2-4	H2-6
	6	6	6	6	6	6	6	6	6	6	6	7	7	6	6
N213V	*	*	*											*	*
L214P	*	*	*												
R259S	*														
K274A	*	*	*	*	*	*	*	*	*	*	*	*	*	*	*
L277R	*	*	*									*	*	*	*
D299E	*		*												
N303H	*	*	*	*	*			*	*		*	*			
I306L	*													*	*
F334Y	*	*	*			*			*			*	*	*	*
P363N			*									*			
G364M												*			
S366T	*														
I367L			*											*	
C391G	*	*	*	*	*	*	*	*	*	*	*	*	*	*	*
G425A	*	*	*												

<sup>a</sup>An asterisk indicates the presence of a mutation. <sup>b</sup>The time (in days) required for colony formation that can be detected by the eye is given below the mutant designation. The same plasmid construct with WT AS allows growth in 2 days.

Table 3. Steady-State Kinetics for Anthranilate Production<sup>a</sup>

	(NH <sub>4</sub> ) <sub>2</sub> SO <sub>4</sub>			PabA/(NH <sub>4</sub> ) <sub>2</sub> SO <sub>4</sub>			PabA/L-glutamine		
	K <sub>choris</sub> (μM)	k <sub>cat</sub> (min <sup>-1</sup> )	k <sub>cat</sub> /K <sub>choris</sub> (M <sup>-1</sup> min <sup>-1</sup> )	K <sub>choris</sub> (μM)	k <sub>cat</sub> (min <sup>-1</sup> )	k <sub>cat</sub> /K <sub>choris</sub> (M <sup>-1</sup> min <sup>-1</sup> )	K <sub>choris</sub> (μM)	k <sub>cat</sub> (min <sup>-1</sup> )	k <sub>cat</sub> /K <sub>choris</sub> (M <sup>-1</sup> min <sup>-1</sup> )
2.6.1	34	0.28	8.2 × 10 <sup>3</sup>	37	0.24	6.4 × 10 <sup>3</sup>	40	0.10	2.6 × 10 <sup>3</sup>
6.6.1	77	0.89	1.2 × 10 <sup>4</sup>	83	0.84	1.0 × 10 <sup>4</sup>	40	0.29	7.2 × 10 <sup>3</sup>
7.6.1	53	0.80	1.5 × 10 <sup>4</sup>	81	0.60	7.4 × 10 <sup>3</sup>	40	0.22	5.6 × 10 <sup>3</sup>
WT AS	25	575	2.3 × 10 <sup>7</sup>				10	740	7.6 × 10 <sup>7</sup>

<sup>a</sup>Errors in K<sub>choris</sub> and k<sub>cat</sub> were less than 20 and 15%, respectively. The reference k<sub>cat</sub>/K<sub>choris</sub> value for the ADCS mutants is that of wild-type ADCS in its cognate reaction using 200 mM NH<sub>4</sub><sup>+</sup> as the source of ammonia, which is 3.3 × 10<sup>4</sup> M<sup>-1</sup> min<sup>-1</sup>. Reaction conditions: 100 mM TEA-HCl (pH 7.8), 100 mM (NH<sub>4</sub>)<sub>2</sub>SO<sub>4</sub>, 5 mM MgCl<sub>2</sub>, and 10–500 μM chorismate.

JW1256-1 transformed with pBAD-trpE grows in 2 days on selection plates. *E. coli* JW1256-1 transformed with pBAD-mutants grew into visible colonies between days 6 and 14. All colonies that grew on the initial selection plates were restreaked onto fresh M9 selection plates to eliminate false positives. True positives were restreaked to measure growth rates. The pabB genes from true positive colonies with reproducible growth times were sequenced to determine the mutations present and confirm that they occur only in the protein coding region. Three mutants that grew within 6 days were isolated from the gene reassembly library, termed 2.6.1, 6.6.1, and 7.6.1 (Table 2).

The five mutations occurring in all three isolates from the first round of selection were shuffled using a megaprimer method to give a new library of ~3000. Eight isolates grew to visible colonies in 6 days and were sequenced. They are included in Table 2 as the “H1” set and show that K274A and C391G are required for activity. Each of the eight mutants also includes either N303H or F334Y but not both.

The same megaprimer method was used to construct a new library of the 15 top-ranked conservation mutations predicted by Janus. From this library of 10<sup>6</sup> transformants, ~200 colonies grew within 1 week. Ten colonies were restreaked; four of these grew and were sequenced. They are presented in Table 2 as the “H2” set. The H1 and H2 isolates were grown on LB medium to test the possibility that toxic compounds synthesized from the mutant enzymes slow growth. All isolates showed visible colonies on LB agar plates within 24 h of incubation at 37 °C.

There are five mutations that occur homogeneously in the first round of selection (K274A, L277R, N303H, F334Y, and C391G), while the second and third rounds have two and four of these same mutations occurring homogeneously. L277R is just outside the Mg<sup>2+</sup> binding site, and the mutation to Arg allows interaction with the metal binding carboxylates. N303H is located in an α-helix next to the Mg<sup>2+</sup> binding Glu302, but pointing away from the active site. F334Y is 14 Å from the active site near the surface of the enzyme. Lastly, C391G is located in the enolpyruvyl side chain binding pocket under Trp390.

**Kinetic Studies.** Steady-state kinetic parameters for TrpE, TrpEG, PabB K274A, 2.6.1, 6.6.1, and 7.6.1 at pH 7.8 are listed in Table 3. Previously, steady-state kinetics for wild-type ADCS gave a K<sub>choris</sub> of 58 ± 8 μM and a k<sub>cat</sub> of 1.9 ± 0.1 min<sup>-1</sup> (k<sub>cat</sub>/K<sub>choris</sub> = 3.3 × 10<sup>4</sup> M<sup>-1</sup> min<sup>-1</sup>) with 200 mM NH<sub>4</sub><sup>+</sup> as the source of ammonia. These values are ~1000-fold lower than that for wild-type AS. We propose that k<sub>cat</sub>/K<sub>M</sub> for ADCS with ammonia as the nitrogen source is the best reference for the catalytic fitness of the isolated mutants because the context for the mutations is ADCS. Although the mutations change the chemistry catalyzed, they are unlikely to alter physical steps such as product dissociation that appear to limit ADCS catalysis.<sup>11</sup>

The mutant ADCS enzymes were assayed for the production of anthranilate using three different sources of ammonia: ammonium ions, ammonium ions in the presence of the glutamidotransferase domain of ADCS (PabA), and ammonia

generated through hydrolysis of L-glutamine via PabA. The PabA/L-glutamine ammonia source gave the lowest  $k_{cat}$  values of the three conditions tested, possibly because of disrupted interactions between the mutants and PabA. The  $k_{cat}$  values for 2.6.1, 6.6.1, and 7.6.1 are 650–2000-fold lower than that of wild-type AS (discussed above), but the  $K_{choris}$  values are only 2–3-fold higher with 200 mM  $\text{NH}_4^+$  as the ammonia source. Both the  $k_{cat}$  and  $K_{choris}$  values for production of anthranilate by all three mutants are remarkably similar to those of wild-type ADCS and its K274A mutant for ADC formation. The largest difference is with 2.6.1, which has a  $k_{cat}/K_{choris}$  value for anthranilate formation that is 25% of the wild-type ADCS value for PABA production. The smallest difference is with 7.6.1, which has a  $k_{cat}/K_{choris}$  value for anthranilate production that is 45% of the wild-type ADCS value for ADC production.

**HPLC Studies.** HPLC chromatograms of reaction mixtures are presented in Figure 5. Reaction products of 2.6.1, 6.6.1, and

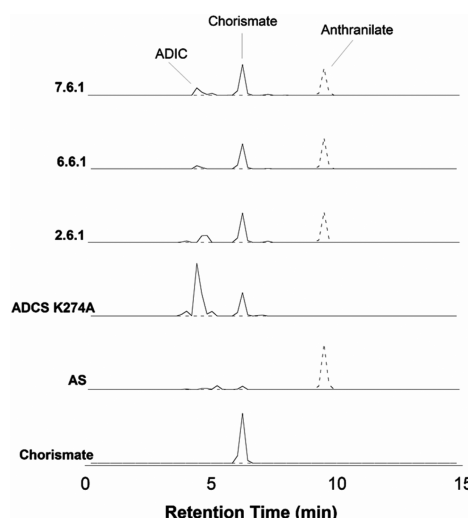


**Figure 5.** HPLC chromatograms of reaction products of PabB K274A, 2.6.1, 6.6.1, 7.6.1, and AS. Chorismate (5 mM) was the substrate in each reaction. HPLC traces for UV detection (solid) and fluorescence (dashed). The two detector signals were not normalized to concentrations.

7.6.1 were analyzed by HPLC to verify the production of anthranilate and to determine if other products were formed. Reactions without enzyme were performed to verify retention times of chorismate and anthranilate, and their stability. Peak assignments were based on comparison of retention times with those of authentic standards. K274A ADCS production of ADIC has been previously reported.<sup>11</sup> Mutants 2.6.1, 6.6.1, and 7.6.1 all produce ADIC and anthranilate. K274A ADCS was previously reported to have no AS activity, which was verified here.<sup>13</sup> Small differences in peak retention times are due to slight variations in chromatographic conditions over the period of time during which the data were collected.

**NMR Analysis.**  $^1\text{H}$  NMR spectra of reactions catalyzed by AS and SS are shown in Figure 6. The splitting pattern of the pyruvate methyl proton signal is an indicator of deuterium incorporation; the presence of a deuterium in the methyl group (i.e.,  $-\text{CH}_2\text{D}$ ) gives a triplet. Both AS (Figure 6A) and SS (Figure 6B) reactions yielded deuterated pyruvate as a product, as evidenced by the triplet at 2.32 ppm. The spectra in Figure 6 also show the presence of fully protiated pyruvate as a singlet at 2.34 ppm, because of  $\text{H}_2\text{O}$  present in the reaction mixtures

(21% for AS and 30% for SS). The fact that fully protiated pyruvate is present at a concentration equal to or greater than that of singly deuterated pyruvate indicates the presence of a substantial solvent isotope effect on the elimination step of the reaction because the  $\text{D}_2\text{O}$  contents of the solvent are 79 and 70% for AS and SS, respectively. An SS-catalyzed reaction in which the enzyme was exchanged into  $\text{D}_2\text{O}$  before being added to the reaction mixture (final  $\text{H}_2\text{O}$  content of 5%) shows a very similar spectrum with the ratio of the fully protiated to monodeuterated product being lower, as expected (Figure 6C). Floss et al. previously reported a solvent isotope effect on pyruvate elimination for the AS-catalyzed reaction,<sup>28</sup> which is confirmed here for AS and SS in the stopped-flow studies reported below. The aromatic regions of the  $^1\text{H}$  NMR spectra clearly show the formation of salicylate by SS and anthranilate by AS. Control reactions in which no enzyme was added showed formation of neither aromatic products nor pyruvate (not shown), while control reactions in which products were incubated with enzyme showed no detectable exchange of pyruvate methyl protons with deuterons from solvent (Figure 6D,E). Therefore, neither AS nor SS catalyzes exchange of deuterium into pyruvate from the product side of the reaction.

Previous work by Kosicki on the nonenzymatic exchange of pyruvate protons with  $\text{D}_2\text{O}$  allows one to estimate the expected extent of nonenzymatic exchange occurring over the 4 h incubation used here.<sup>29</sup> Table 1 of that work presents data from which a rate constant of  $2 \times 10^{-6} \text{ s}^{-1}$  is calculated for proton exchange in the presence of 200 mM potassium phosphate ( $\text{pD}$  7.2), 20 mM  $\text{MgCl}_2$ , and 2 mM EDTA. The buffer and  $\text{Mg}^{2+}$  concentrations are both ~10-fold higher than in the experiments presented here, and each of these components catalyzes proton exchange. Therefore, this rate constant is a 10–100-fold overestimate of that expected under our conditions. After incubation for 4 h, the calculated extent of exchange is 2.5% using their rate constant, which corresponds to 15  $\mu\text{M}$  monodeuterated pyruvate. Correcting for a 10-fold lower expected rate constant under our conditions gives 15  $\mu\text{M}$  monodeuterated pyruvate expected in the control reactions presented in panels D and E of Figure 6. We expect this to be below the noise level of the experiment.

**Stopped-Flow Analysis.** Figure 7 presents the results of rapid mixing experiments with AS and chorismate. The enzyme was in excess, under single-turnover conditions. The formation of anthranilate shows a lag phase, as expected for the AS mechanism in which chorismate is first converted to ADIC followed by conversion of ADIC to anthranilate (the fluorescent product) via pyruvate elimination. From these data, the rate constants assigned to ADIC formation and pyruvate elimination are  $17.5 \pm 1.3$  and  $8.0 \pm 0.6 \text{ s}^{-1}$ , respectively, consistent with the steady-state  $k_{cat}$  value reported at a slightly higher pH in Table 3. The  $\text{D}_2\text{O}$  solvent KIEs obtained from the data are  $1.4 \pm 0.1$  for conversion of chorismate to ADIC and  $2.0 \pm 0.2$  for pyruvate elimination. Similar reactions with SS gave rate constants for isochorismate formation and pyruvate elimination of  $0.12 \pm 0.01$  and  $0.030 \pm 0.002 \text{ s}^{-1}$ , respectively, and corresponding  $\text{D}_2\text{O}$  solvent KIEs of  $1.5 \pm 0.1$  and  $1.4 \pm 0.1$ , respectively (data not shown). For comparison, previous studies of ADCS in the absence of PabA gave a value of  $6.3 \pm 0.2 \text{ s}^{-1}$  for addition of Lys274 to C2 of chorismate to give the covalent intermediate, yet the  $k_{cat}$  value for the overall reaction with  $(\text{NH}_4)_2\text{SO}_4$  as the nitrogen source is only  $0.032 \pm 0.002 \text{ s}^{-1}$ . Similarly, reactions of ADCS with PabA and glutamine as the nitrogen source gave a value of  $57 \pm$

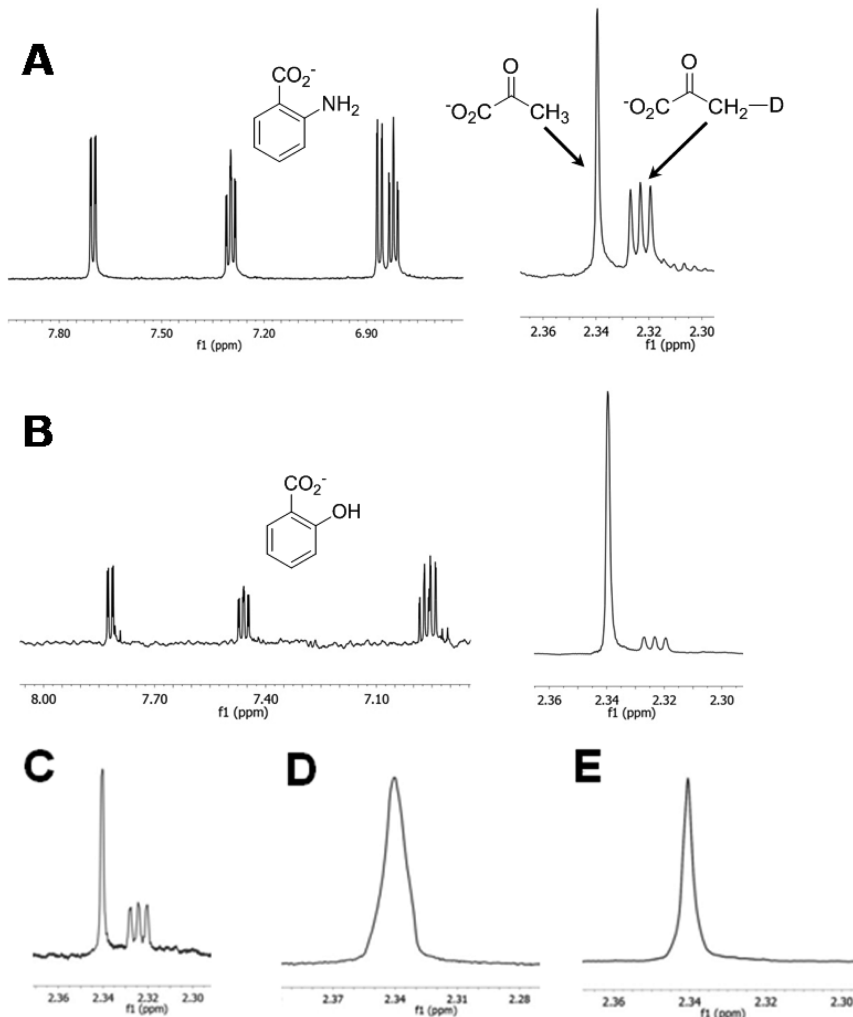


**Figure 6.**  $^1\text{H}$  NMR spectra of chorismate reactions with (A) AS in 89%  $\text{D}_2\text{O}$  and (B) SS in 70%  $\text{D}_2\text{O}$ . The presence of a deuterium in the pyruvate methyl group (i.e.,  $-\text{CH}_2\text{D}$ ) gives a triplet at  $\sim 2.32$  ppm. (C) Pyruvate region of an SS reaction in which the enzyme stock solution was exchanged into  $\text{D}_2\text{O}$  before being added to the reaction mixture. The final reaction mixture has 95%  $\text{D}_2\text{O}$ . The pattern is the same as in panel B, but the ratio of fully protiated to monodeuterated pyruvate decreases. (D) Pyruvate region of a reaction mixture in which SS was incubated with 6 mM products in  $\text{D}_2\text{O}$ . (E) Pyruvate region of a reaction mixture in which AS was incubated with 6 mM products in  $\text{D}_2\text{O}$ .

$3\text{ s}^{-1}$  for addition of Lys274 to C2 of chorismate and  $0.53 \pm 0.02\text{ s}^{-1}$  for  $k_{\text{cat}}$ .

**Computational Modeling.** The X-ray structures of ADCS, AS, IS, SS, and ADIC synthase (PhzE) were used to model chorismate into the active sites based on bound products or product analogues. Figure 8 shows the modeled structures of K274A-ADIC and 7.6.1-ADIC before and after simulated annealing energy minimization. The initial equatorial structure of ADIC bound to K274A is converted to axial after simulated annealing energy minimization. Conversely, the initial axial structure of ADIC bound to 7.6.1 is converted to equatorial after simulated annealing energy minimization. Likewise, the structures of AS, SS, ADIC synthase, and IS show a strong preference for one conformation of the appropriate chorismate derivative or the other (Figure 9). AS and SS, which like 7.6.1 catalyze pyruvate elimination, favor the equatorial conformation. On the other hand, ADIC synthase and IS, which do not catalyze pyruvate elimination, favor the axial conformation. This correlation implies that catalysis of pyruvate elimination involves controlling the conformation of the substrate for the elimination reaction.

The X-ray structure of IS with isochorismate bound (PDB entry 3HWO) has isochorismate in a nearly axial conformation. The C-C bonds in the ring have lengths of  $\sim 1.4\text{ \AA}$  (except the C2-C3 bond), which suggests that the force field parameters used for refinement of isochorismate were not correct because double bonds should be  $\sim 1.3\text{ \AA}$  long and single bonds should be  $\sim 1.5\text{ \AA}$  long. The appropriate bond orders were manually adjusted, and the YASARA automated parameter assignment tool was used to derive AMBER03 parameters for isochorismate, which were confirmed manually after simulated annealing calculations on isochorismate alone. When the protein and crystallographic waters were held fixed and isochorismate was energy minimized using steepest descent, the conformation of isochorismate spontaneously changed to fully axial.

The energy differences between the axial and equatorial conformers of chorismate and its derivatives relevant to this study are listed in Table 4. The energy differences were calculated for both water and methanol as solvents to gauge the dielectric dependence of the equilibrium constant. In water, the equatorial conformer of chorismate is favored  $\sim 4$ -fold, while that for isochorismate is favored  $\sim 40$ -fold. In contrast, the axial

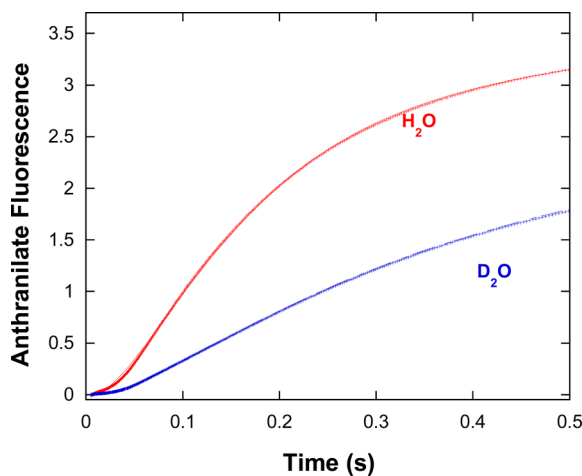


**Figure 7.** Stopped-flow analysis of the AS reaction in  $\text{H}_2\text{O}$  and  $\text{D}_2\text{O}$ . Each trace is the average of three reactions. Note the lag phase at the beginning of the reactions. The data were fit to the time course for C in the reaction  $\text{A} \rightarrow \text{B} \rightarrow \text{C}$ , which represents conversion of chorismate to ADIC followed by pyruvate elimination. Anthranilate was detected by fluorescence ( $\lambda_{\text{ex}} = 313 \text{ nm}$ ;  $\lambda_{\text{em}} > 340 \text{ nm}$ ). The rate constants for the reactions in  $\text{H}_2\text{O}$  are  $17 \pm 1$  and  $8.0 \pm 0.6 \text{ s}^{-1}$  for the first and second steps, respectively. The  $\text{D}_2\text{O}$  KIEs obtained from these data are  $1.4 \pm 0.1$  and  $2.0 \pm 0.2$ , respectively. Similar reactions with SS gave rate constants of  $0.12 \pm 0.01$  and  $0.030 \pm 0.002 \text{ s}^{-1}$  in  $\text{H}_2\text{O}$  for the first and second steps, respectively, and  $\text{D}_2\text{O}$  KIEs of  $1.5 \pm 0.1$  and  $1.4 \pm 0.1$ , respectively. Reaction conditions:  $50 \mu\text{M}$  enzyme,  $40 \mu\text{M}$  chorismate,  $50 \text{ mM}$  potassium phosphate ( $\text{pH}/\text{pD} 7.0$ ),  $5 \text{ mM}$   $\text{MgCl}_2$ , and  $20 \text{ mM}$  L-glutamine.

conformer of ADIC is favored in the protonated and unprotonated states by 13- and 140-fold, respectively.

## ■ DISCUSSION

The mechanism by which pyruvate elimination is catalyzed by AS, SS, and other structurally homologous chorismate enzymes has occupied enzymologists for many years. The current literature trend is to interpret them as pericyclic reactions in which the methine carbon of the enolpyruvyl side chain accepts the C2 hydrogen simultaneously with C3–O bond cleavage.<sup>7,8,18</sup> This has the attraction of being a rather novel enzyme catalytic mechanism and has as precedent the mechanism of PchB, an isochorismate pyruvate lyase homologous to chorismate mutase. Both of the latter enzymes appear to catalyze pericyclic reactions.<sup>30–38</sup>

The fly in the ointment for the pericyclic proposal, for AS at least, is that there is strong literature evidence for an acid/base mechanism. In 1970, Floss et al. and Tamir and Srinivasan published independent papers showing that the AS-catalyzed elimination of pyruvate occurs with incorporation of a solvent-derived proton into the pyruvate methyl group.<sup>21,28</sup> The only reasonable interpretation of these data is that the AS-catalyzed elimination of pyruvate occurs through an acid/base mechanism, not through a pericyclic one in which the C2 hydrogen of ADIC would be obligatorily transferred to the pyruvate methyl group. More recently, Zwahlen et al. performed similar experiments with SS, conducting reactions in  $\text{D}_2\text{O}$  with protiated chorismate, with different results.<sup>8</sup>  $^1\text{H}$  NMR analysis of these reactions showed that the pyruvate produced was fully protiated as expected for a pericyclic reaction, not deuterated as expected for an acid/base reaction. The results presented here in Figure 6 agree with the previous work on AS and are at odds

with the results of Zwahlen et al. on SS-catalyzed reactions. The  $\text{D}_2\text{O}$  solvent isotope effects presented in Figure 7 (and evident in Figure 6) are also at odds with their results.

The determination of X-ray structures for these enzymes and the availability of many homologous sequences from genome projects have added a new dimension to the mechanistic search. The common sense premise is that there should be acid/base residues present near the enolpyruvyl side chain in the active sites of AS and SS (which catalyze pyruvate elimination) and absent in the active sites of ADCS, ADIC synthase, and IS (which do not catalyze pyruvate elimination). The absence of such reaction-specific residues in the enzyme active sites therefore reasonably motivated searches for other fundamentally different types of catalytic mechanisms, with the pericyclic mechanism being the most attractive given the precedent of chorismate mutase and PchB-catalyzed pericyclic reactions on chorismate and isochorismate, respectively.

In this work, a different approach was taken. It was decided that a definitive answer to the question of how these important enzymes control elimination activity would best be found by converting a pyruvate elimination-deficient enzyme into a pyruvate elimination-proficient one and analyzing the basis of the introduced activity. To do so, we predicted the mutations required using the Janus program that we developed for enzyme interconversion.<sup>23</sup>

In principle, the conservation and covariation scores reported by Janus predict the relative importance of individual residues to enzyme interconversion-based multiple-sequence alignments, but the total number of mutations necessary for conversion is not currently predicted. Previously, the 35 top-ranked aspartate aminotransferase-to-tyrosine aminotransferase predictions included mutations that were deleterious to catalysis and created a very large library of  $\sim 10^{10}$  that could not be fully screened. Given these prior results, the number of mutations in this work was kept small to generate a library that could be fully screened. Inclusion of the 15 top-ranked conservation predictions gave a library size of  $2^{15}$  ( $\sim 33000$ ).

The Janus-predicted mutations succeeded in converting ADCS into an AS-like enzyme. The steady-state  $k_{\text{cat}}$  for 7.6.1, the best mutant, is  $0.013 \text{ s}^{-1}$ . Compared to  $0.032 \text{ s}^{-1}$  for the wild-type ADCS conversion of chorismate into ADC under similar conditions, 7.6.1 is 40% as fast as ADCS under saturating conditions.<sup>11</sup> The formation of the covalent intermediate, chemically the most difficult step in the ADCS reaction, is  $\sim 100$ -fold faster than  $k_{\text{cat}}$ . Two steps follow covalent intermediate formation of ADCS: reaction with ammonia to give enzyme-bound product and product dissociation. Like covalent intermediate formation in ADCS and ADIC formation in AS, addition of ammonia to the covalent intermediate to generate enzyme-bound ADC is expected to be fast, suggesting that product dissociation is rate-limiting for the wild-type enzyme.<sup>11</sup> Indeed, X-ray structures of *E. coli* ADCS show a large-scale conformational change of residues 270–310, which close over the active site to sequester reactants.<sup>6</sup> One might reasonably expect the same rate-limiting step for the mutants isolated here given the small number of mutations in each, although further kinetic analysis would be required to demonstrate this unequivocally.

The Janus-predicted mutations for introducing pyruvate elimination activity into ADCS (Table 1) do not place acid/base functional groups near the enolpyruvyl side chain in the active site. In fact, Cys391 is the closest residue in the ADCS active site that might act as an acid to protonate the methine

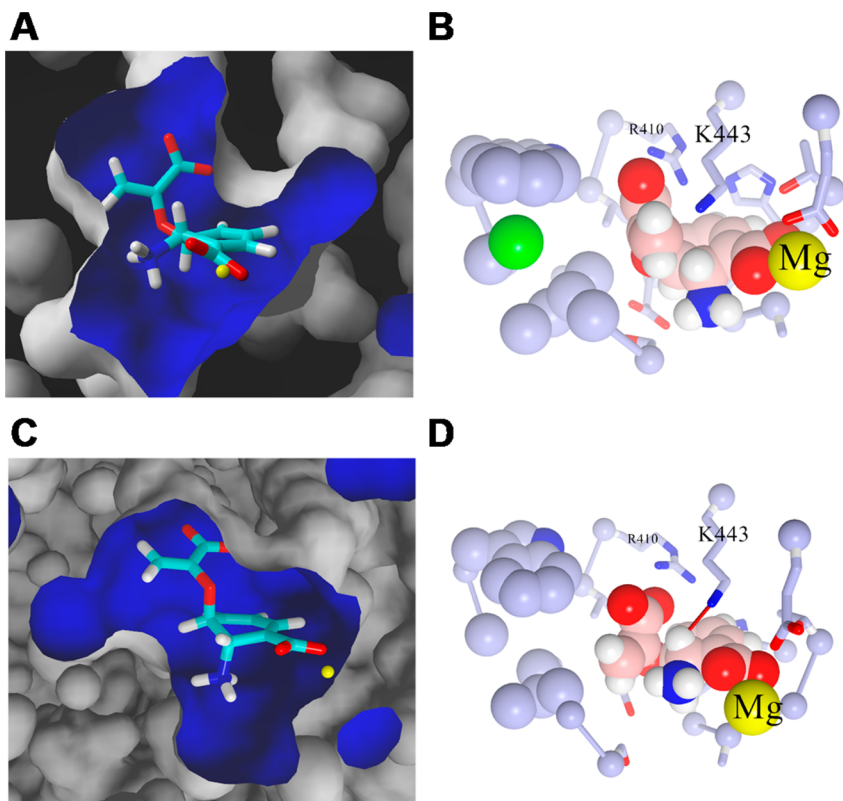


**Figure 8.** (A) Molecular surface of K274A shown with the equatorial conformer of ADIC docked before simulated annealing energy minimization. (B) Active site structure of K274A after simulated annealing energy minimization with ADIC starting in the equatorial conformation. The final conformation is axial. (C) Molecular surface of the 7.6.1 mutant shown with the axial conformer of ADIC docked before simulated annealing energy minimization. (D) Active site structure of 7.6.1 after simulated annealing energy minimization with ADIC starting in the axial conformation. The final conformation is equatorial.

carbon of the pyruvate leaving group, and it is changed to Gly in all three mutants isolated. Therefore, an alternative explanation for activity of the mutants was sought.

A structure for the 7.6.1 mutant was constructed by homology modeling in YASARA based on that of WT ADCS. The model was superimposed on the structure of AS with benzoate bound, and either axial or equatorial ADIC was modeled into the active site of 7.6.1 based on the benzoate ligand in the AS active site. The docked ADIC structures were energy minimized by simulated annealing from 298 to 10 K; both final structures had the equatorial conformer (Figure 8). A similar exercise with K274A ADCS resulted in only the axial conformation after energy minimization (Figure 8). The most obvious source of the conformational differences is the increase in the volume of the pocket near the enolpyruvyl side chain in the 7.6.1 mutant. The C391G and I367L mutations combine to make room for the enolpyruvyl side chain in the equatorial conformation. The C391G mutation allows Trp390 to move down and out of the way in the view of Figure 8. The I367L mutation moves the side chain methyl group to the  $\gamma$  position, further increasing the size of the pocket.

The enticing results with K274A ADCS and 7.6.1 motivated further computational work with other structurally and mechanistically homologous chorismate enzymes. Figure 9 presents results for AS, SS, ADIC synthase, and IS. In each case, simulated annealing energy minimizations were started from both conformers of the potential elimination substrate, and each led to the same final conformation. AS and SS (which catalyze pyruvate elimination) give the equatorial conformer,

while ADIC synthase and IS (which do not catalyze pyruvate elimination) give the axial conformation. On the basis of these results, we hypothesize that this family of enzymes determines elimination reaction specificity by controlling the conformation of the bound substrate. This proposal is illustrated schematically in Figure 10.

In this model, the equatorial conformation is active for elimination because in addition to placing the C2–H bond parallel to the  $\pi$  orbitals of the conjugated diene/carboxylate  $\pi$  system, it also places the C2–H bond within striking distance of a completely conserved active site lysine (Lys443 in ADCS and Lys424 in SS) to act as a general base catalyst. Conversely, the axial conformation is elimination inactive because the advantageous stereoelectronic effects are not in play and the C2–H bond is not accessible to the lysine.

Given the charge neutralization of the carboxylate group by  $Mg^{2+}$ , the extended conjugation of the diene/carboxylate system, and the absence of an obvious acid to act in concert at the enolpyruvyl leaving group, it seems most likely that the elimination reaction is an  $E1_{cb}$  type with a carbanionic intermediate. This was previously proposed for the  $S_N2''$  reaction of SS leading to isochorismate based on quantum mechanics/molecular mechanics studies.<sup>39</sup> The last step of the reaction is protonation of the leaving group on C3 to give pyruvate, incorporating a solvent-derived proton into the methyl group. Given that there is no other obvious candidate for an acid catalyst, we propose that the conserved active site lysine also plays this role. The stability of the carbanion in the  $E1_{cb}$  mechanism allows time for the now-protonated lysine to

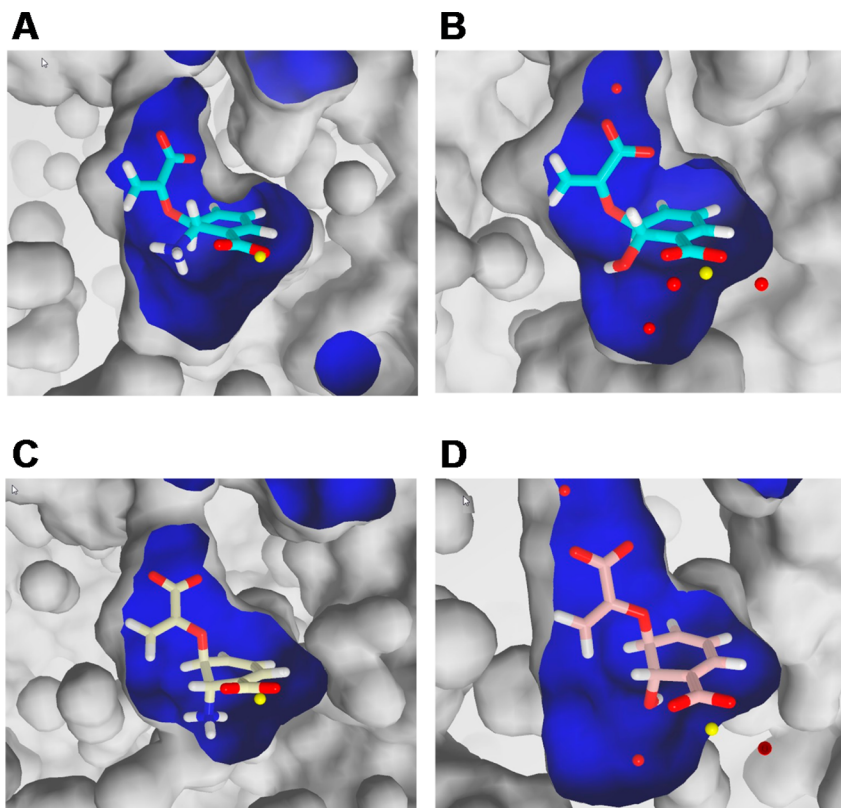


**Figure 9.** Molecular surfaces of (A) AS, (B) SS, (C) ADIC synthase, and (D) IS around the active site after simulated annealing energy minimization. In all cases, the simulations were initiated with the opposite conformer of that shown. An additional set of calculations starting from the conformers shown here did not lead to conformational alterations in the substrate. Thus, the conformations shown here are likely to be the most stable in the active sites.

**Table 4. Conformational Energy Differences (kilocalories per mole) for Chorismate and Derivatives<sup>a</sup>**

substrate	$\Delta E$ (axial-equatorial) in water	$\Delta E$ (axial-equatorial) in methanol
chorismate	0.81	0.08
isochorismate	2.2	2.4
ADIC (protonated)	-1.5	-1.2
ADIC (unprotonated)	-2.9	-2.7

<sup>a</sup>Calculated using Gaussian09 at the HF/6-311+G(d,p) level of theory using the PCM solvent model.

move into position to act as an acid catalyst on the enolpyruvyl leaving group. This step could occur either through direct protonation of the methine carbon of the leaving group or through protonation of the ether oxygen leading to the enol tautomer of pyruvate, which would tautomerize to pyruvate. Both of these routes would give incorporation of a solvent-derived proton into the methyl group. The solvent isotope effect would arise by transfer of a solvent-derived proton from the lysine  $\epsilon$ -amino group to the enolpyruvyl leaving group.

This mechanistic hypothesis answers two puzzling questions concerning ADCS. First, why is it that the covalent intermediate with Lys274 bound to C2 is not susceptible to pyruvate elimination and thereby enzyme inactivation in the course of its normal reaction? The answer lies in the observation that Lys274 can reasonably add to C2 only from the axial position, leaving the C2-H bond unsusceptible to deprotonation by Lys443. Second, given the fact that pyruvate elimination is the next step in PABA biosynthesis, why does

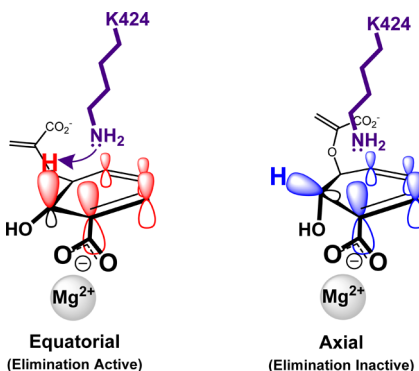


**Figure 10.** Schematic illustration of conformational control of pyruvate elimination. The axial conformation both maximizes stereoelectronic activation via orbital overlap with the conjugated  $\pi$  system and presents the C2-H bond to the active site lysine (Lys424 in SS and Lys443 in the ADCS mutants isolated here), which acts as a base catalyst for deprotonation.

ADCS not catalyze pyruvate elimination from bound ADC? Here, the answer appears to be that Lys443 simply cannot access the C4-H bond to act as a base catalyst for deprotonation, because of the presence of Arg410 and its interaction with the enolpyruvyl carboxylate.

Importantly, the literature contains additional data on chorismate analogues that provide unequivocal evidence against a pericyclic elimination mechanism, at least in the case of AS.<sup>40</sup> The analogues shown in Table 5 show significant activity with AS in anthranilate formation yet are incapable of undergoing a

Table 5. Activities of Chorismate Analogues with AS<sup>a</sup>

Structure	Activity vs. Chorismate
	15%
	4%
	3%

<sup>a</sup>From ref 40.

pericyclic elimination reaction because the double bond in the leaving group is absent. The only reasonable possibility for elimination with these is an E1<sub>cb</sub> acid/base mechanism with protonation of the leaving group on the ether oxygen, given the poor nature of the leaving groups and the resonance stabilization of the carbanion.

Conformational control of acid/base-catalyzed pyruvate elimination nicely unifies previous and current isotopic studies of pyruvate elimination catalyzed by AS and SS, as well as a large body of sequence and structure information. The NMR results (Figure 6) show that, as expected, a solvent-derived proton is incorporated into the pyruvate methyl group in reactions catalyzed by AS and SS, while both the NMR and the rapid kinetic results (Figure 7) confirm the presence of solvent isotope effects on the acid-catalyzed S<sub>N</sub>2" step and the acid/base-catalyzed pyruvate elimination step. The only piece of information that cannot be reconciled with the proposed mechanism is the report by Zwahlen et al. that SS-catalyzed reactions in D<sub>2</sub>O yield pyruvate with no detectable deuterium in the methyl group. The results reported in Figure 6 were reproducible over multiple experiments for both enzymes and were conducted under conditions identical to those reported by Zwahlen et al. Given that more than 40 years ago two independent laboratories reported results for AS identical to those reported here, and that conservation of mechanism is generally observed in enzyme families, the weight of the evidence favors conformational control of acid/base-catalyzed pyruvate elimination for this enzyme family as a whole rather than a pericyclic mechanism.

## AUTHOR INFORMATION

### Corresponding Author

\*E-mail: mdtony@ucdavis.edu. Phone: (530) 754-5282. Fax: (530) 752-8995.

### Notes

The authors declare no competing financial interest.

## ACKNOWLEDGMENTS

We thank Robert W. Mertz for providing assistance with running Janus, Justin B. Siegel for allowing use of his plate reader and for help with small-scale protein purification, and Andrew Ferreira and Michael Donald for help collecting NMR data.

## ABBREVIATIONS

AS, anthranilate synthase; ADCS, 4-amino-4-deoxychorismate synthase; SS, salicylate synthase; IS, isochorismate synthase; ADC, 4-amino-4-deoxychorismate; ADIC, 2-amino-2-deoxyisochorismate; PCR, polymerase chain reaction.

## REFERENCES

- Walsh, C. T., Liu, J., Rusnak, F., and Sakaitani, M. (1990) Molecular Studies on Enzymes in Chorismate Metabolism and the Enterobactin Biosynthetic-Pathway. *Chem. Rev.* 90, 1105–1129.
- Herrmann, K. M., and Weaver, L. M. (1999) The Shikimate Pathway. *Annu. Rev. Plant Physiol. Plant Mol. Biol.* 50, 473–503.
- Dosselaere, F., and Vanderleyden, J. (2001) A metabloic node in action: Chorismate-utilizing enzymes in microorganisms. *Crit. Rev. Microbiol.* 27, 75–131.
- O'Callaghan, D., Maskell, D., Liew, F. Y., Easmon, C. S., and Dougan, G. (1988) Characterization of aromatic- and purine-dependent *Salmonella typhimurium*: Attention, persistence, and ability to induce protective immunity in BALB/c mice. *Infect. Immun.* 56, 419–423.
- Morollo, A. A., and Eck, K. J. (2001) Structure of the cooperative allosteric anthranilate synthase from *Salmonella typhimurium*. *Nat. Struct. Biol.* 8, 243–247.
- Parsons, J. F., Jensen, P. Y., Pachikara, A. S., Howard, A. J., Eisenstein, E., and Ladner, J. E. (2002) Structure of *Escherichia coli* aminodeoxychorismate synthase: Architectural conservation and diversity in chorismate-utilizing enzymes. *Biochemistry* 41, 2198–2208.
- Lamb, A. L. (2011) Pericyclic reactions catalyzed by chorismate-utilizing enzymes. *Biochemistry* 50, 7476–7483.
- Zwahlen, J., Kolappan, S., Zhou, R., Kisker, C., and Tonge, P. J. (2007) Structure and Mechanism of MbtI, the Salicylate Synthase from *Mycobacterium tuberculosis*. *Biochemistry* 46, 954–964.
- Sridharan, S., Howard, N., Kerbarh, O., Blaszczyk, M., Abell, C., and Blundell, T. L. (2010) Crystal structure of *Escherichia coli* enterobactin-specific isochorismate synthase (EntC) bound to its reaction product isochorismate: Implications for the enzyme mechanism and differential activity of chorismate-utilizing enzymes. *J. Mol. Biol.* 397, 290–300.
- Ye, Q. Z., Liu, J., and Walsh, C. T. (1990) para-Aminobenzoate Synthesis in *Escherichia coli*: Purification and Characterization of PABB as Aminodeoxychorismate Synthase and Enzyme-X as Aminodeoxychorismate Lyase. *Proc. Natl. Acad. Sci. U.S.A.* 87, 9391–9395.
- He, Z., and Toney, M. D. (2006) Direct detection and kinetic analysis of covalent intermediate formation in the 4-amino-4-deoxychorismate synthase catalyzed reaction. *Biochemistry* 45, 5019–5028.
- Spraggon, G., Kim, C., Nguyen-Huu, X., Yee, M. C., Yanofsky, C., and Mills, S. E. (2001) The structures of anthranilate synthase of *Serratia marcescens* crystallized in the presence of (i) its substrates, chorismate and glutamine, and a product, glutamate, and (ii) its end-product inhibitor, L-tryptophan. *Proc. Natl. Acad. Sci. U.S.A.* 98, 6021–6026.
- He, Z., Stigers Lavoie, K. D., Bartlett, P. A., and Toney, M. D. (2004) Conservation of mechanism in three chorismate-utilizing enzymes. *J. Am. Chem. Soc.* 126, 2378–2385.
- Li, Q., Mavrodi, D. V., Thomashow, L. S., Roessle, M., and Blankenfeldt, W. (2011) Ligand binding induces an ammonia channel in 2-amino-2-deoxyisochorismate (ADIC) synthase PhzE. *J. Biol. Chem.* 286, 18213–18221.

(15) Huang, X. Y., Holden, H. M., and Raushel, F. M. (2001) Channeling of substrates and intermediates in enzyme-catalyzed reactions. *Annu. Rev. Biochem.* **70**, 149–180.

(16) Raushel, F. M., Thoden, J. B., and Holden, H. M. (2003) Enzymes with molecular tunnels. *Acc. Chem. Res.* **36**, 539–548.

(17) Hiraka, Y. (2002) Invasiveness of *Pseudomonas aeruginosa* and its role in diversity of *Pseudomonas* Infectious Diseases. *Acta Med. Nagasaki.* **47**, 89–96.

(18) Kerbarh, O., Chirgadze, D. Y., Blundell, T. L., and Abell, C. (2006) Crystal structures of *Yersinia enterocolitica* salicylate synthase and its complex with the reaction products salicylate and pyruvate. *J. Mol. Biol.* **357**, 524–534.

(19) Culbertson, J. E., and Toney, M. D. (2013) Expression and characterization of PhzE from *P. aeruginosa* PAO1: Aminodeoxychorismate synthase involved in pyocyanin and phenazine-1-carboxylate production. *Biochim. Biophys. Acta* **1834**, 240–246.

(20) Floss, H. G., Onderka, D. K., and Zalkin, H. (1970) Mechanism of the anthranilate synthetase reaction. Evidence against an intramolecular hydrogen transfer. *Biochim. Biophys. Acta* **206**, 449–456.

(21) Tamir, H., and Srinivasan, P. R. (1970) Studies of the mechanism of anthranilate synthase reaction. *Proc. Natl. Acad. Sci. U.S.A.* **66**, 547–551.

(22) Ziebart, K. T., and Toney, M. D. (2010) Nucleophile Specificity in Anthranilate Synthase, Aminodeoxychorismate Synthase, Isochorismate Synthase, and Salicylate Synthase. *Biochemistry* **49**, 2851–2859.

(23) Addington, T. A., Mertz, R. W., Siegel, J. B., Thompson, J. M., Fisher, A. J., Fisher, A. J., Filkov, V., Fleischman, N. M., Suen, A. A., Zhang, C., and Toney, M. D. (2013) Janus: Prediction and ranking of mutations required for functional interconversion of enzymes. *J. Mol. Biol.* **425** (8), 1378–1389.

(24) Gibson, F. (1963) Chorismic Acid: Purification and some Chemical and Physical Studies. *Biochem. J.* **90**, 256–261.

(25) Krieger, E., Koraiemann, G., and Vriend, G. (2002) Increasing the precision of comparative models with YASARA NOVA: A self-parameterizing force field. *Proteins* **47**, 393–402.

(26) Krieger, E., Darden, T., Nabuurs, S. B., Finkelstein, A., and Vriend, G. (2004) Making optimal use of empirical energy functions: Force-field parameterization in crystal space. *Proteins* **57**, 678–683.

(27) Krieger, E., Dunbrack, R. L., Jr., Hooft, R. W., and Krieger, B. (2012) Assignment of protonation states in proteins and ligands: Combining pK<sub>a</sub> prediction with hydrogen bonding network optimization. *Methods Mol. Biol.* **819**, 405–421.

(28) Floss, H. G., Onderka, D. K., and Zalkin, H. (1970) Mechanism of the anthranilate synthetase reaction. Evidence against an intramolecular hydrogen transfer. *Biochim. Biophys. Acta* **206**, 449–456.

(29) Kosicki, G. W. (1968) Oxaloacetate decarboxylase from cod. Catalysis of hydrogen-deuterium exchange in pyruvate. *Biochemistry* **7**, 4310–4314.

(30) Choutko, A., Eichenberger, A. P., van Gunsteren, W. F., and Dolenc, J. (2013) Exploration of swapping enzymatic function between two proteins: A simulation study of chorismate mutase and isochorismate pyruvate lyase. *Protein Sci.* **22**, 809–822.

(31) Olucha, J., Ouellette, A. N., Luo, Q., and Lamb, A. L. (2011) pH Dependence of catalysis by *Pseudomonas aeruginosa* isochorismate-pyruvate lyase: Implications for transition state stabilization and the role of lysine 42. *Biochemistry* **50**, 7198–7207.

(32) Luo, Q., Meneely, K. M., and Lamb, A. L. (2011) Entropic and enthalpic components of catalysis in the mutase and lyase activities of *Pseudomonas aeruginosa* PchB. *J. Am. Chem. Soc.* **133**, 7229–7233.

(33) Marti, S., Andres, J., Moliner, V., Silla, E., Tunon, I., and Bertran, J. (2009) Mechanism and plasticity of isochorismate pyruvate lyase: A computational study. *J. Am. Chem. Soc.* **131**, 16156–16161.

(34) Luo, Q., Olucha, J., and Lamb, A. L. (2009) Structure-function analyses of isochorismate-pyruvate lyase from *Pseudomonas aeruginosa* suggest differing catalytic mechanisms for the two pericyclic reactions of this bifunctional enzyme. *Biochemistry* **48**, 5239–5245.

(35) Kong, Y., Ma, J., Karplus, M., and Lipscomb, W. N. (2006) The allosteric mechanism of yeast chorismate mutase: A dynamic analysis. *J. Mol. Biol.* **356**, 237–247.

(36) Zhang, X., and Bruice, T. C. (2005) A definitive mechanism for chorismate mutase. *Biochemistry* **44**, 10443–10448.

(37) Hur, S., and Bruice, T. C. (2002) The mechanism of catalysis of the chorismate to prephenate reaction by the *Escherichia coli* mutase enzyme. *Proc. Natl. Acad. Sci. U.S.A.* **99**, 1176–1181.

(38) Guo, H., Cui, Q., Lipscomb, W. N., and Karplus, M. (2001) Substrate conformational transitions in the active site of chorismate mutase: Their role in the catalytic mechanism. *Proc. Natl. Acad. Sci. U.S.A.* **98**, 9032–9037.

(39) Ferrer, S., Marti, S., Moliner, V., Tunon, I., and Bertran, J. (2012) Understanding the different activities of highly promiscuous MbtI by computational methods. *Phys. Chem. Chem. Phys.* **14**, 3482–3489.

(40) Walsh, C. T., Erion, M. D., Walts, A. E., Delany, J. J., III, and Berchtold, G. A. (1987) Chorismate aminations: Partial purification of *Escherichia coli* PABA synthase and mechanistic comparison with anthranilate synthase. *Biochemistry* **26**, 4734–4745.